PERGAMON

International Journal of Heat and Mass Transfer 43 (2000) 825–838

International Journal of HEAT and MASS TRANSFER

www.elsevier.com/locate/ijhmt

Natural convection around horizontal downward-facing plate with rectangular grooves: experiments and numerical simulations

C.E. Kwak, T.H. Song*

Department of Mechanical Engineering, Korea Advanced Institute of Science and Technology, Kusong-dong, Yusong-gu, Taejon 305-701, South Korea

Received 21 August 1998; received in revised form 19 February 1999

Abstract

Laminar natural convection around a two-dimensional horizontal downward-facing plate with rectangular grooves was studied experimentally and numerically. A Mach–Zehnder interferometer was used in the experiment and the local Nusselt numbers at each groove surface (outer, upper, left side and right side surfaces) were measured quantitatively from interferograms. In some cases (grooves of some aspect ratios with a low Rayleigh number), the increase of the total heat transfer rate from grooved surface may not be sufficiently large in spite of the increased surface area. As revealed by the numerical analysis for the given conditions, secondary recirculation flows are usually observed in the groove. The protrusions prevent the main flow from flowing into the groove and cause recirculations. As they happen, the heat transfer rate at the upper surfaces of the groove is significantly smaller than that at the outer surface. The effect of Rayleigh number for each aspect ratio was also studied. The results are summarized using the average Nusselt number versus Rayleigh number correlations. The correlations may be used in selecting proper aspect ratio and dimension.

Keywords: Natural convection; Horizontal downward-facing plate; Grooved plate interferometer experiment; Numerical simulation

1. Introduction

Recently, electronic systems and equipment have been demanded for smaller sizes and higher capability. The distance between chips is becoming shorter and the integration rate of components is getting higher. The electric power consumption thus increases considerably, while the size of electronic equipment diminishes. The chip level power density has increased from 20 to 60 W/cm^2 during past 15 years. It is expected to reach 100 W/cm^2 in the near future [1]. It eventually increases the temperature of electronic systems and causes failure of electronic circuits. Increase of the power necessitates proper heat dissipation methods from the electronic components.

Various cooling modules and the problems associated with electronic equipment cooling are reviewed in detail by Incropera [2]. The cooling methods may be classified into air-cooling, air–liquid hybrid cooling, indirect liquid cooling, and direct liquid cooling (immersion cooling). They can be also classified to natural convection, forced convection and boiling in accordance with the employed physical phenomena [3].

* Corresponding author. Tel.: +82-42-869-3032; fax: +82-42-869-3210.

E-mail address: thsong@sorak.kaist.ac.kr (T.H. Song).

0017-9310/00/$ - see front matter
PII: S0017-9310(99)00164-7

Nomenclature

b	depth of the experimental specimen
c_p	specific heat (J/kg K)
Gr_W	Grashof number ($= g\beta\Delta T W^3/\nu^2$)
g	gravitational acceleration (9.81 m/s)
H	depth of the groove (m)
h	local heat transfer coefficient (W/m^2 K)
$\bar{h}$	average heat transfer coefficient ($\frac{Q}{L(T_w-T_\infty)}$; W/m^2 K)
k	thermal conductivity (W/m K)
L	total horizontal length of the specimen (m)
n	refractive index of air
$\overline{Nu_L}$	average Nusselt number based on the total length $L(\bar{h}L/k)$
Nu_W	local Nusselt number (hW/k)
$\overline{Nu_W}$	average Nusselt number based on the pitch length $W(\bar{h}W/k)$
P	pressure (Pa)
$P*$	dimensionless pressure ($= (P+\rho_\infty gy)/(\rho_\infty \nu^2/W^2)$)
Pr	Prandtl number ($= \nu/\alpha$)
q''	local heat flux (W/m^2)
Q	total heat transfer rate from the fin per unit depth (W/m)
Ra_W	Rayleigh number ($Gr_W \cdot Pr$)
T	temperature (K)
ΔT	temperature difference between the wall and the surrounding ($= T_w - T_\infty$; K)
u	x-direction velocity (m/s)
v	y-direction velocity (m/s)
W	length of a pitch ($W_1 + W_2$; m)
W_1	width of the groove (m)
W_2	width of the protrusion (m)
α	thermal diffusivity ($= k/\rho c_p$; m^2/s)
β	thermal expansion coefficient (K^{-1})
θ	dimensionless temperature ($= (T-T_\infty)/(T_w - T_\infty)$)
ν	kinematic viscosity of the fluid (m^2/s)
ρ	density of the fluid (kg/m^3)

Subscripts

g	groove
w	wall
∞	surrounding

Superscript

*	dimensionless quantity

The cooling system using natural convection has the advantage of low noise and high reliability. When used in air, it is generally limited to electronic components of low power density. High power density may be handled by immersion cooling, a liquid natural convection system for the next generation electronic circuits.

To enhance heat transfer from the chip, grooved plate is frequently used as a typical extended surface geometry. Various heat transfer situations can be met depending on the flow and/or the groove orientations. Vertical mounting with the grooves parallel to the gravity is the best installation method for natural convection, for which the performance and optimal fin spacing are well documented by Bejan, together with some other situations [4]. However, due to other reasons, many different installations are inevitably employed. A situation, though not very efficient but difficult-to-analyze, is when the natural convective flow is perpendicular to the groove orientation. The authors have previously reported the performance of grooved plates with vertical mounting and horizontal groove orientation [5], and with upward-facing orientation [6]. This paper is about the third situation when the grooved plate is facing downward so that buoyant flow comes up to the center then sweeps to the edge as shown in Fig. 1.

Reviewing the previous related works, the early studies until the 1970s on natural convection from a horizontal downward-facing plate have been initiated mainly by experimental methods. Experimental and analytical integral methods have been used until 1980. Use of numerical method such as Finite Difference Method (FDM) has initiated since the early 1980s. Before citing the earlier works, it is appropriate to comment here; there is a confusion in the literature regarding the characteristic length in the average Nusselt and Rayleigh numbers. Some authors suggest the correlation based on the half length and others based on the total length L. Every cited correlation here is adjusted as based on the total length. Fishenden and Saunders [7] present a dimensionless correlation for square plates in the form $Nu = 0.31Ra^{1/4}$ ($10^5 < Ra < 10^{10}$). Kadambi and Drake [8] recorrelate the original Sounder et al.'s data based on laminar boundary layer theory with 1/5th power to the Rayleigh number. Fujii and Imura [9] experimentally investigate natural convection from a horizontal downward-facing plate and they suggest the correlation, $Nu = 0.58Ra^{1/5}$ ($10^6 < Ra < 10^{11}$). The thermal condition at the wall is somewhere between uniform heat flux and isothermal condition. Aihara et al. [10] measure the velocity field near the downward-

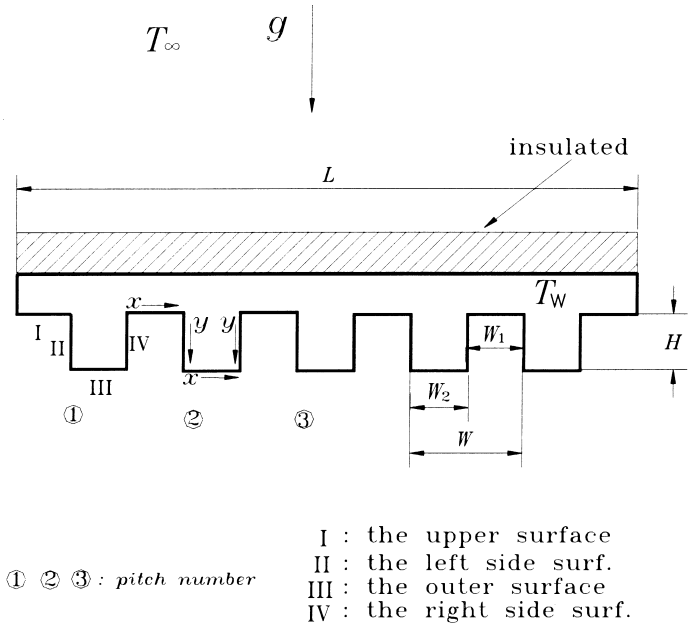

Fig. 1. Notations of the horizontal downward facing rectangular grooved fin.

facing surface utilizing trajectories of fine particles. Also, the validity of Gill et al.'s [11] theoretical conclusion that similarity solutions cannot be obtained for free convection along a downward facing, isothermal, heated surface, is experimentally confirmed in both the velocity and temperature fields in their study. Wagner [12] applies integral method to natural convection from a heated plate facing downward and shows the correlation in the form $Nu = 0.66Ra^{1/5}$. He assumes that the boundary layer thickness is nearly zero at the edges. Clifton and Chapman [13] analyze heat transfer from a finite plate theoretically. They propose that the thickness of boundary layer at the leading edge is not zero, but it corresponds to the condition of minimum specific mechanical energy there. Fuji et al. [14] study laminar natural convection from heated horizontal flat plates facing downwards with uniform surface heat flux, using an approximate integral method. Solutions for an infinite strip, a circular plate and a rectangular plate are obtained for any Prandtl number. They give the correlation for an infinite strip in the form $Nu = 0.59Ra^{1/5}$ ($Pr = 0.7$). Restrepo and Glicksman [15] study natural convection from a heated square plate with three different edge conditions. The average heat transfer coefficient for a heated edge ($Nu = 0.68Ra^{1/5}$) is 17% greater than the heat transfer coefficient for a cooled edge ($Nu = 0.587Ra^{1/5}$). The heat transfer coefficient for a heated horizontal extensions ($Nu = 0.41Ra^{1/5}$) is 30% below that for a cooled edge. Hatfield and Edwards [16] use flat plates with bare edges, and with approximately adiabatic extensions around the edges to investigate edge effects. The following correlation including the length of adiabatic extension is proposed.

$$Nu = C_1\left[1 + C_2L/b\right]\left[(1+X)^{3m} - X^{3m}\right]Ra^m \tag{1}$$

where, $X = C_3Ra^m + C_4(L_a/L)^p$. The seven coefficients C_1, C_2, C_3, C_4, m, n, and p are empirical constants. Symbol L is short side length of the plate and L_a is length of the adiabatic extension, and b is long side length of the plate. Goldstein and Lau [17] study laminar natural convection from a horizontal plate using a finite difference analysis and experiments. The correlations ($3 \times 10^2 < Ra < 6 \times 10^4$) are reported in the form $Nu = 0.65Ra^{1/5}$ (experiment) and $Nu = 0.69Ra^{1/5}$ (FDM). The horizontal extension and vertical wall are used to investigate influence of the plate edge extensions. The insulated horizontal extension causes a limited reduction in the heat transfer and the effect is larger in downward-facing geometry than in upward-facing geometry. Until today, the studies on natural convection from horizontal downward-facing rectangular fin arrays are scarcely performed in contrast to upward rectangular fin arrays. The main difference of two geometries is that the former has flow flowing into the center from the edge and the latter has vertical buoyant plume at the plate center flow a chimney.

In this paper, both of experimental and numerical researches are made to study natural convection from heated horizontal grooved plates facing downward. A Mach–Zehnder interferometer is used to visualize the

Table 1
Dimensions of the models

Case	$W = W_1 + W_2$ (mm)	H/W	W_2/W
1 (Square groove)	14	0.5	0.5
2 (Shallow groove)	14	0.25	0.5
3 (Deep groove)	14	1	0.5
4 (Wide groove)	15	7/15	0.2

temperature distribution and the interferogram is compared with the numerical results using a modified SIMPLER code with pressure boundary condition. The local heat transfer rates and flow fields are calculated to investigate physical phenomena around the groove. The effects of Rayleigh number and the aspect ratio of grooves are studied and the amounts of total heat transfer enhancement of each case are calculated.

2. Experimental study

An experimental model of the downward rectangular grooved fin is shown in Fig. 1. The depth of the test section perpendicular to the page is 0.2 m, while the total width is 7–7.5 cm. It, thus, exhibits highly two-dimensional behavior. The plate is made of aluminum and has five rectangular protrusions, and its surface is heated isothermally due to its high thermal conductivity. Heating wire is uniformly attached on the backside of the specimen and it is heated using a dc power supply. To prevent heat dissipation from the backside, an insulation material is adhered. Symbol H denotes the depth of the groove, W_1 is the width of the groove, W_2 is the width of the protruded top surface and W, the pitch length, is the sum of W_1 and W_2. The experiments are performed varying the aspect ratios H/W and W_2/W. The actual sizes of the models are shown in Table 1.

The Mach–Zehnder interferometer used in the experiment is schematically shown in Fig. 2. Isothermal lines are visualized using infinite fringe frames and the distribution of Nusselt numbers at the surfaces is measured using finite fringe frames [18]. After the interferogram is taken with a camera, the picture is magnified to the size 10 in. × 8 in. It is then analyzed with a digitizer having a 500 dpi resolution. It is assumed, for the convenience of data processing, that the temperature gradient of the refractive index dn/dT is constant. For verification of the experimental results, the average Nusselt number over the horizontal flat plate facing downwards is measured and compared with other studies. The obtained value is 5.6% higher than that of Sounders [7] and 7.8% lower than the correlation of Hatfield [16] for $Ra_L = 1.9 \times 10^6$. Therefore, the real value is somewhere between Sounders' and Hatfield's results. Square specimen are used in Sounders' experiment and the aspect ratio (L/b; see Eq. (1)) of this experiment is 0.385. Hatfield reports that the proposed correlation (1) fits the data of other researches within ±10% error. And thus, our experimental results are within the error bound of other studies and it confirms the validity of the experimental results. The greatest error comes from the

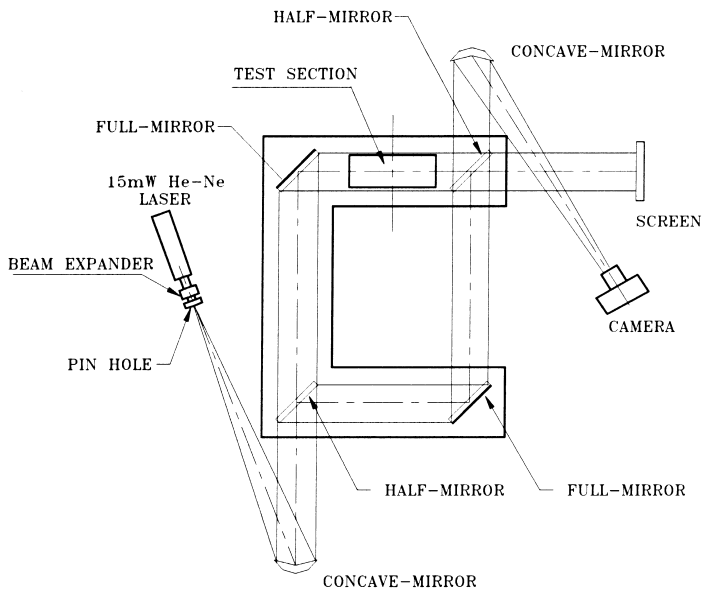

Fig. 2. The Mach–Zehnder interferometer used in experiments.

uncertainties in reading the interferogram, i.e., the temperature gradient near the wall is very high and the fringes have fairly large thickness. With all these uncertainties, the error of experimental Nusselt number is $\pm 9\%$.

3. Numerical study

The interferograms give information only about the temperature distributions. To find the velocity field and to further verify the experimental results, numerical simulations are also performed.

The dimensionless governing equations are as follows:

$$\frac{\partial u^*}{\partial x^*} + \frac{\partial v^*}{\partial y^*} = 0 \tag{2}$$

$$u^* \frac{\partial u^*}{\partial x^*} + v^* \frac{\partial u^*}{\partial y^*} = \frac{\partial^2 u^*}{\partial x^{*2}} + \frac{\partial^2 u^*}{\partial y^{*2}} - \frac{\partial P^*}{\partial x^*} \tag{3}$$

$$u^* \frac{\partial v^*}{\partial x^*} + v^* \frac{\partial v^*}{\partial y^*} = \frac{\partial^2 v^*}{\partial x^{*2}} + \frac{\partial^2 v^*}{\partial y^{*2}} - \frac{\partial P^*}{\partial y^*} + Gr_W \theta \tag{4}$$

$$u^* \frac{\partial \theta}{\partial x^*} + v^* \frac{\partial \theta}{\partial y^*} = \frac{1}{Pr}\left(\frac{\partial^2 \theta}{\partial x^{*2}} + \frac{\partial^2 \theta}{\partial y^{*2}} \right) \tag{5}$$

The Boussinesq approximation has been used by introducing $P = P^* \rho_\infty (v^2/W^2) - P_\infty$ with $\partial P_\infty / \partial y = -\rho_\infty g$ and the employed dimensionless quantities are defined as:

$$x^* = \frac{x}{W}, \quad y^* = \frac{y}{W}, \quad u^* = \frac{uW}{v}, \quad v^* = \frac{vW}{v},$$
$$\theta = \frac{T - T_\infty}{T_w - T_\infty}, \quad Gr_W = \frac{g\beta (T_w - T_\infty) W^3}{v^2} \quad \text{and} \quad Pr = \frac{v}{\alpha}. \tag{6}$$

The boundary conditions are given as follows:

$$u^* = 0 \quad \text{and} \quad v^* = 0 \text{ at the surfaces of the fin} \tag{7}$$

$$p^* = 0 \text{ at the bottom, left and right boundaries} \tag{8}$$

$$\theta = 1 \text{ at the surface of the fin, and } \frac{\partial \theta}{\partial y^*} = 0 \text{ at the bottom boundary} \tag{9}$$

In Eqs. (8) and (9), the bottom boundary is a far location that is twelve times the depth of a groove away from the fin. The right computational boundary is at the right side of the last protrusion and the left boundary is at the left side of the first.

In a natural convection problem, velocities can not be prescribed at the boundaries. Thus, the pressure boundary condition (8) is applied here. A SIMPLER code [19] is modified for pressure boundary condition. See Ref. [5] for detailed modification method. Underrelaxation of boundary velocity and pressure is made to make the computation stable.

When the Nusselt number (either local or average) and the heat flux q'' are defined as follows,

$$Nu_W = \frac{hW}{k},$$

$$q'' = h(T_w - T_\infty), \tag{10}$$

They are found to be dependent on the following variables.

$$Nu_W = f(Gr_W, Pr, H/W, W_2/W, \dots) \tag{11}$$

In many situations, the above equation is further simplified as

$$Nu_W = f(Ra_W, H/W, W_2/W, \dots). \tag{12}$$

where $Ra_W = Gr_W \cdot Pr$.

Correlations of experimental data for fluids with $Pr \geq 0.7$ may be accurately expressed by Eq. (12) [20]. In this study, a constant Prandtl number 0.71 is taken and Eq. (12) is employed, indeed.

4. Verification of the numerical simulation

Firstly, grid dependence is examined to minimize the numerical uncertainty. The calculated variables using current grids (81×38) are compared with those using a finer 169×74 mesh for the square groove. The difference of total heat transfer rate between them is at most 3%. Compromising between the computational cost and the accuracy, the current mesh is considered appropriate.

Secondly, the average heat transfer rate for a flat plate is computed and compared with that of Hatfield [16]. Only about 2% discrepancy is found.

Lastly, to demonstrate the accuracy of numerical result of the downward facing plate with grooves, the average Nusselt number of square groove for $Ra_W = 1.14 \times 10^4$ is compared with that of the interferometric experiment. Both results agree well with each other within 3% error. Also, the distributions of the numerical local Nusselt numbers and the experimental ones have the same tendency and their values agree well with each other except for the corner of the protrusion.

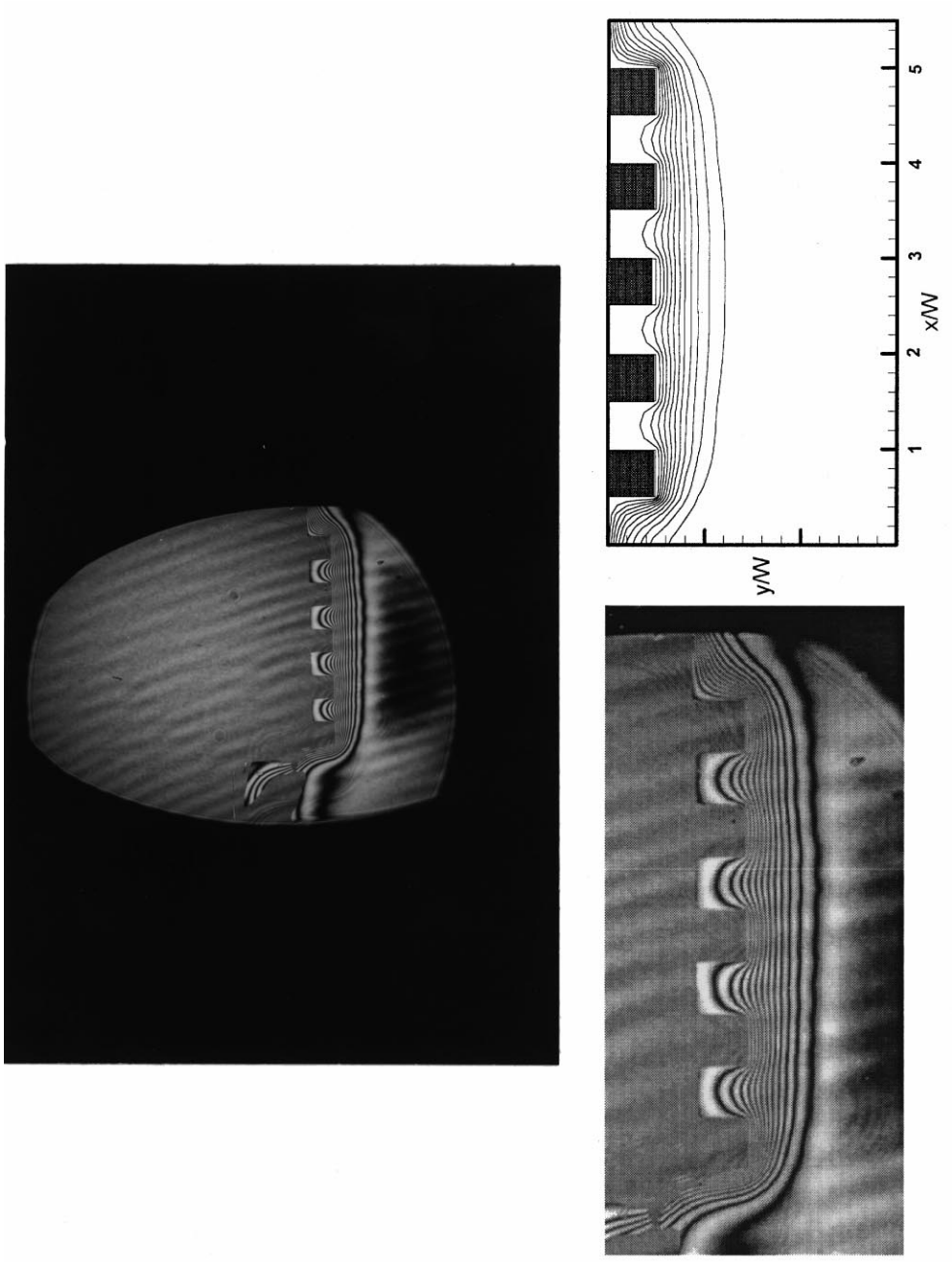

Fig. 3. Comparison of isotherms around a grooved plate (square groove, $Ra_W = 1.14 \times 10^4$).

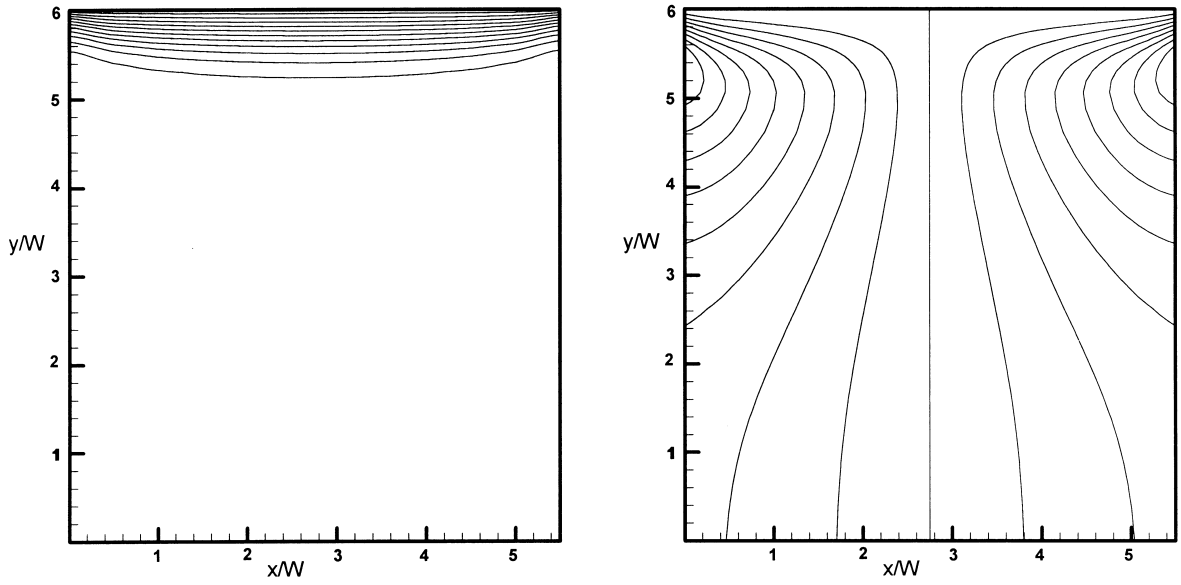

Fig. 4. Isotherms and streamlines of horizontal downward facing flat plate for $Ra_W = 1.14 \times 10^4$.

Since the local heat transfer rates near the corner of the protrusion increase rapidly, experimental measurement is very difficult and the errors of the measured values are large. As mentioned earlier, the numerical results are slightly better in accuracy. The experimental and numerical isotherms are shown in Fig. 3. They agree very well with each other both qualitatively and quantitatively. Since the numerical results are considered better in accuracy than the experimental results and since the experimental results include partly three-dimensional effects, quantitative evaluations hereafter are based on numerical results. All the four cases of Table 1 are calculated and the results are compared. Since the geometry is an important design parameter while the overall size is roughly fixed, the relative performances of different grooves need to be discriminated by directly comparing the heat transfer rates. The Rayleigh number Ra_W is varied as 1.14×10^4, 1.14×10^5, 1.14×10^6 and 1.14×10^7. Note that $L = 5.5W$ so that $Ra_L = 166Ra_W$.

5. Results and discussion

The average Nusselt numbers of a horizontal downward-facing flat plate are numerically calculated and correlated to use as the reference case. The correlation is obtained as follows:

$$\overline{Nu_L} = 0.67Ra_L^{1/5} \quad 1.9 \times 10^6 \leq Ra_L \leq 1.9 \times 10^9 \tag{13}$$

This correlation is nearly identical with those of Wagner [12], Aihara [10] and Restrepo [15]. The isotherms and streamlines for the flat plate with $Ra_W = 1.14 \times 10^4$ ($Ra_L = 1.9 \times 10^6$) are shown in Fig. 4. The thickness of the boundary layer is not zero but finite at the edges, and it reaches maximum at the center. The flow rises toward the center and goes out to the edges.

The isotherms for the four groove geometries of Table 1 are shown in Fig. 5 when Ra_W is 1.14×10^4. Generally, the closer to the center the location of the groove is, the thicker is the thermal boundary layer just like in a flat plate. The outer parts of the protrusion have dense isotherms and those in the groove are sparse. The wall heat flux in the groove is thus much lower than that at the tip of the protrusion. Isothermal lines of shallow and wide grooves penetrate from the ambient into the groove more deeply than the other cases. For these two cases, the groove aspect ratio H/W_1 is smaller than the other cases. The local Nusselt numbers are shown in Fig. 6 for square groove with $Ra_W = 1.14 \times 10^4$. The local Nusselt numbers is the greatest at the outer surface (III) of the groove. At the left side (II) and right side surface (IV), it increases from the inner corner to the outer edge. At the deep upper surface (I) of the groove, it is very small. It has a local maximum at the center and decreases at the corners for the second and the third grooves. And the

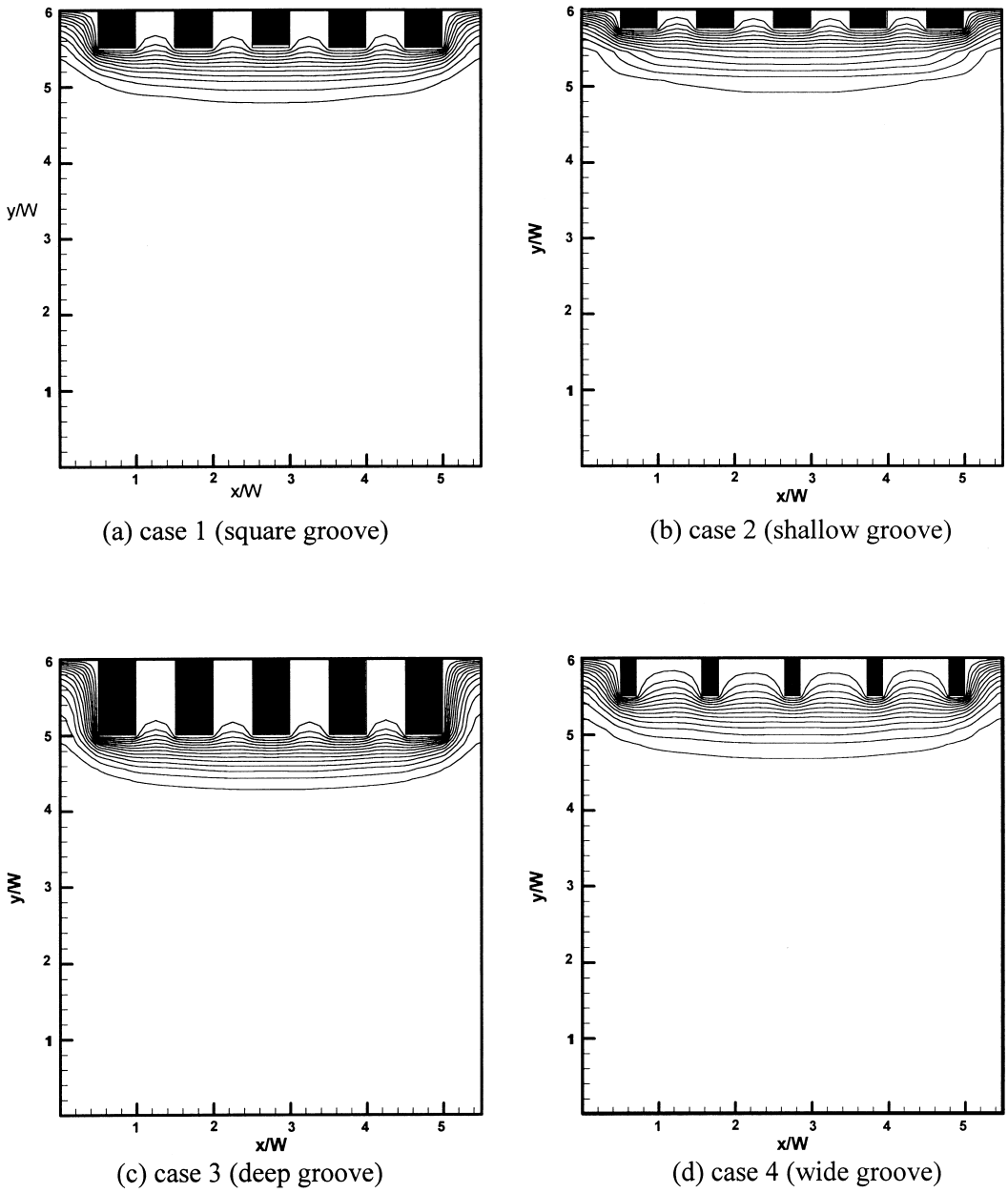

Fig. 5. Isotherms for the four geometries ($Ra_W = 1.14 \times 10^4$).

larger the pitch numbering is (meaning close to the center; see Fig. 1), the smaller is the local Nusselt number. The heat transfer rates of three pitches in the left only are shown since the physical phenomena are symmetrical about the center. The local Nusselt numbers of the upper and the left side surface of pitch 1 are very high, since those surfaces are not in grooves but freely exposed near the edge. The distribution pattern of Nusselt number for the other cases (shallow, deep groove and thin protrusion) is also similar. However, shallow groove and thin protrusion have greater Nusselt number at the upper surface (I) and deep groove has a smaller value there. The heat transfer rate at the upper surface (I) is too small to contribute to the total heat transfer rate except for the wide groove.

The pattern of Nusselt number distribution in the groove can be easily understood when the flow pattern

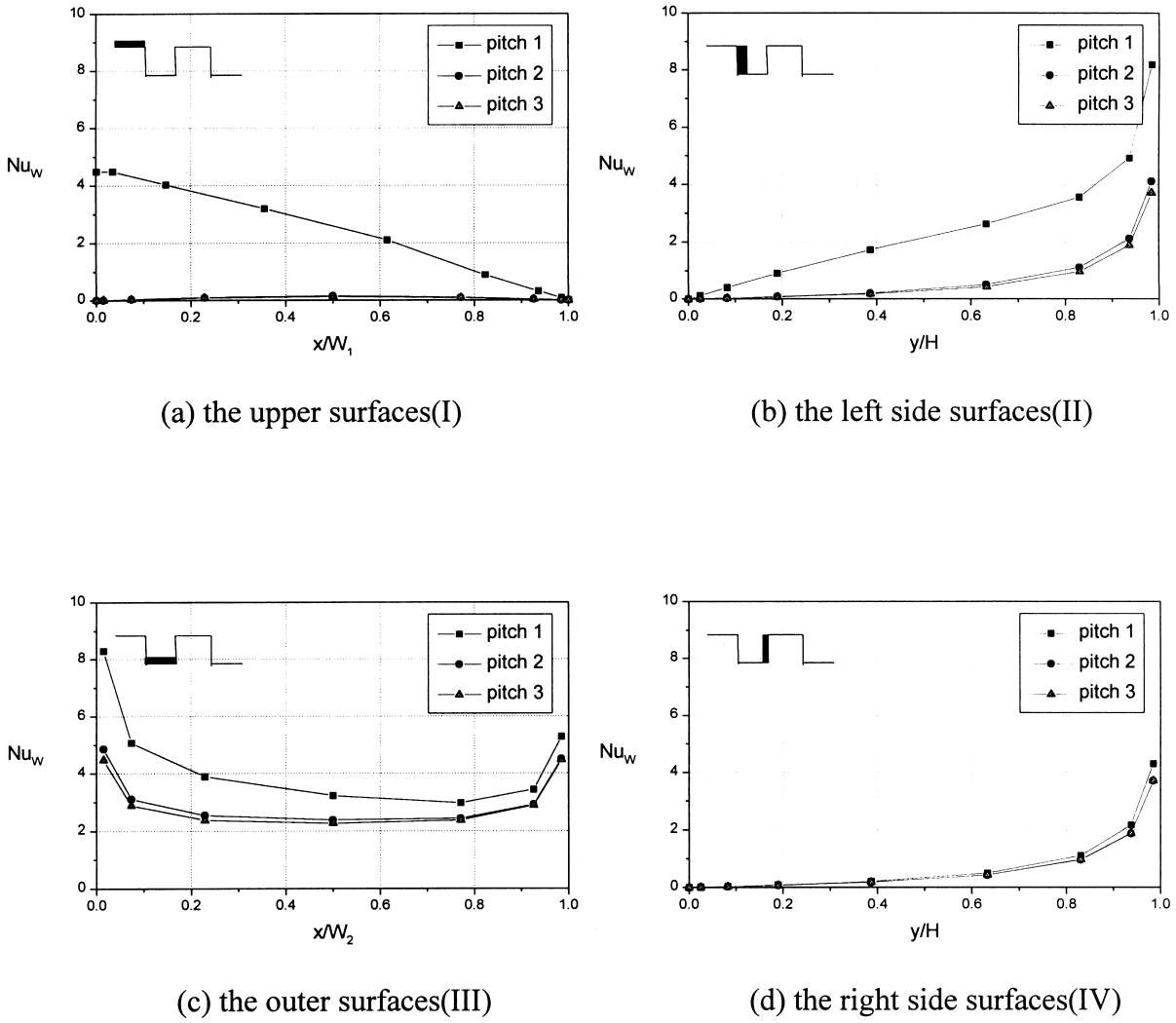

Fig. 6. Distribution of Nu_W at each surface of a pitch for $Ra_W = 1.14 \times 10^4$ (square groove) (see Fig. 1 for the pitch and surface numbering).

in the groove is known. Streamlines of each case are shown in Fig. 7 for $Ra_W = 1.14 \times 10^4$. Note that the streamlines in the groove are drawn with very fine interval of the stream function. Indeed, velocities in the groove are very small. The streamlines in the groove vividly visualize the recirculations. A weak recirculation flow is generated near the right side surface of the protrusion for the left part about the center. The protrusions prevent the main flow from flowing into the groove and cause the recirculations in the groove. For this reason, the heat transfer rate at the bottom surface is very small and so is the Nusselt number. When the groove is very deep (see Fig. 7(c)), main flow rarely penetrates into the grooves and the Nusselt number at the upper surface becomes even smaller.

For the cases of Fig. 7, the total heat transfer rate is the largest for deep groove. It is about 51% larger than that of flat plate. For other geometries, it is smaller in the sequence, square groove (24%), wide groove (13%) and shallow groove (10%). The increases of the total heat transfer rates of the wide and shallow grooves are not large although the exposed area is much greater than flat plate. Those are mainly because the size of the outer tip which has the maximum heat transfer coefficient is very small for the wide groove and the size of the side surfaces is small for the shallow groove.

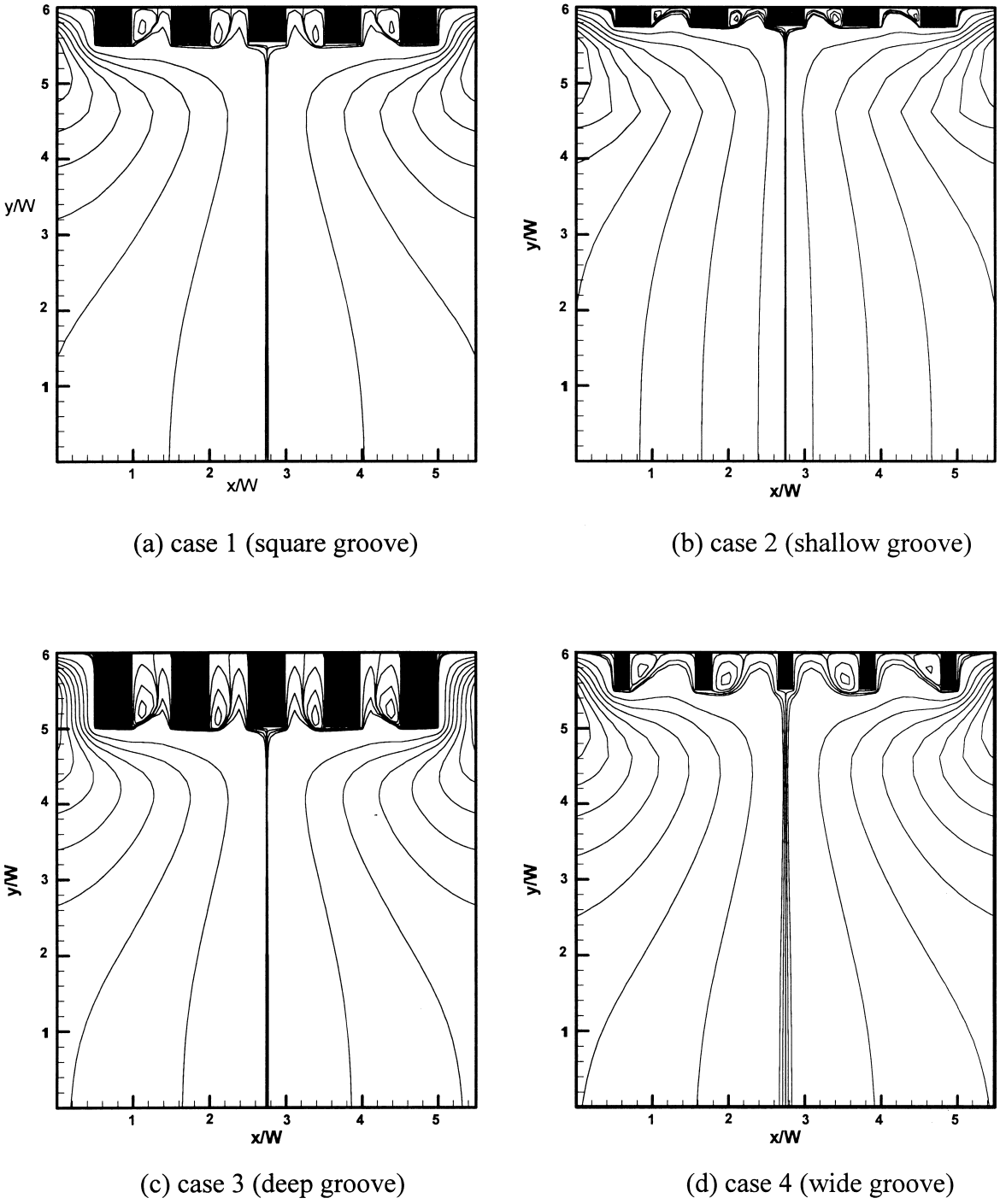

Fig. 7. Streamlines for the four geometries ($Ra_W = 1.14 \times 10^4$).

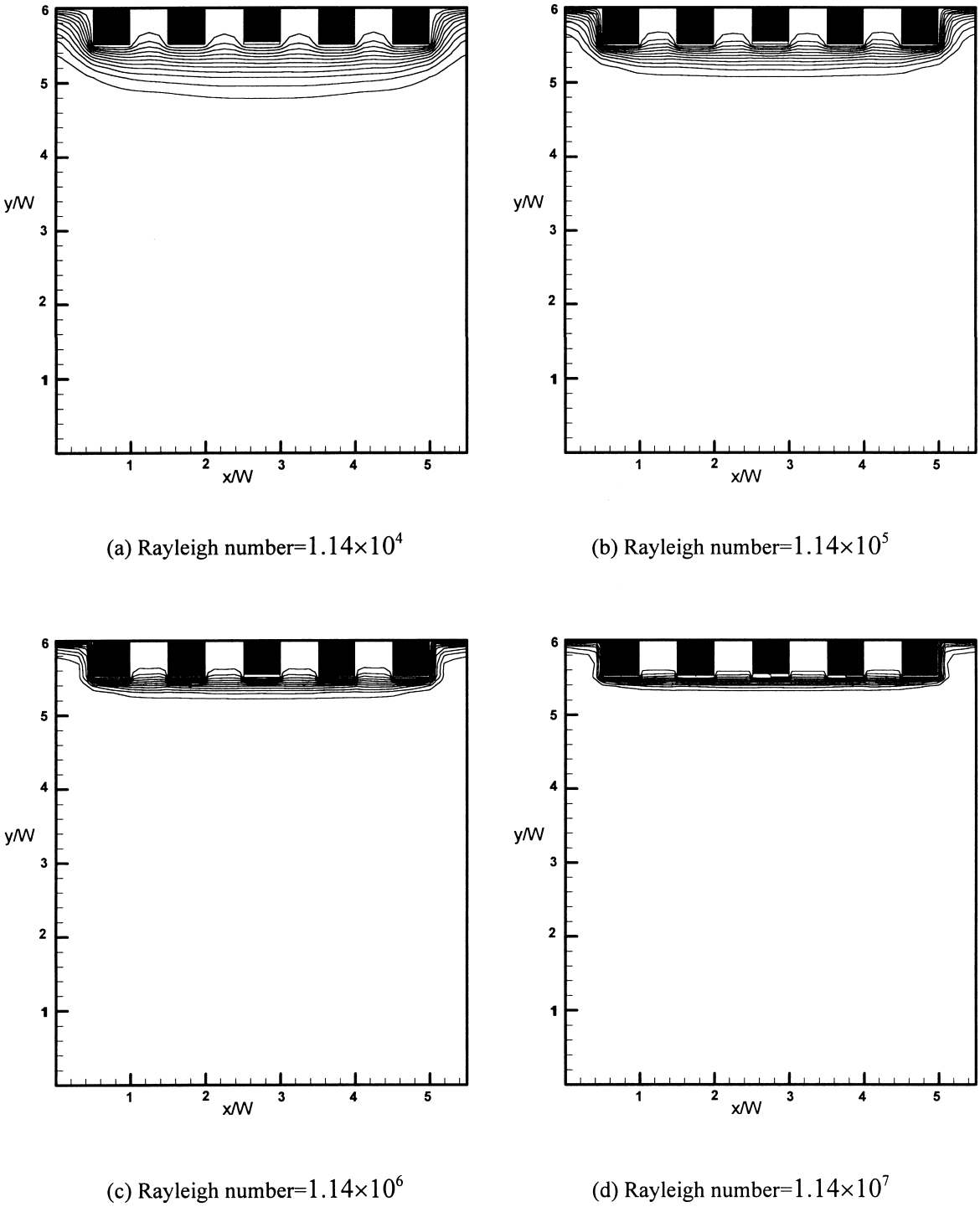

(a) Rayleigh number=1.14×10^4

(b) Rayleigh number=1.14×10^5

(c) Rayleigh number=1.14×10^6

(d) Rayleigh number=1.14×10^7

Fig. 8. Isotherms when varying Ra_W (square groove).

Table 2
Dimensionless heat transfer rate for each case varying $Ra_W(Q/k(T_w - T_\infty))$

	$Ra_W = 1.14 \times 10^4$	$Ra_W = 1.14 \times 10^5$	$Ra_W = 1.14 \times 10^6$	$Ra_W = 1.14 \times 10^7$
Flat plate	11.9	18.7	29.7	48.6
Square groove	14.7	25.2	44.5	80.4
Shallow groove	13.1	22.5	37.7	64.4
Deep groove	18.0	31.8	57.1	104.6
Wide groove	13.5	23.1	40.9	73.4

The isotherms for $Ra_W = 1.14 \times 10^4$, 1.14×10^5, 1.14×10^6 and 1.14×10^7 in square groove are shown in Fig. 8 to see the effect of Ra_W. Though Ra_W increases from (a) to (d), the isotherms and streamline do not penetrate into the groove deeply. Only the thickness of boundary layer near the outer surfaces decreases. The dimensionless total heat transfer rate for variation of Ra_W is shown in Table 2 for all cases and for a flat plate. Total heat transfer rates of all cases are larger than that of a flat plate when $Ra_W \geq 1.14 \times 10^5$. The higher Ra_W is, the larger is the enhancement of heat transfer. The increasing rate, though not very high, is higher for grooved plate than for a flat plate. Thus, the advantage by increasing the surface area is visualized when the Rayleigh number is larger than about 10^6.

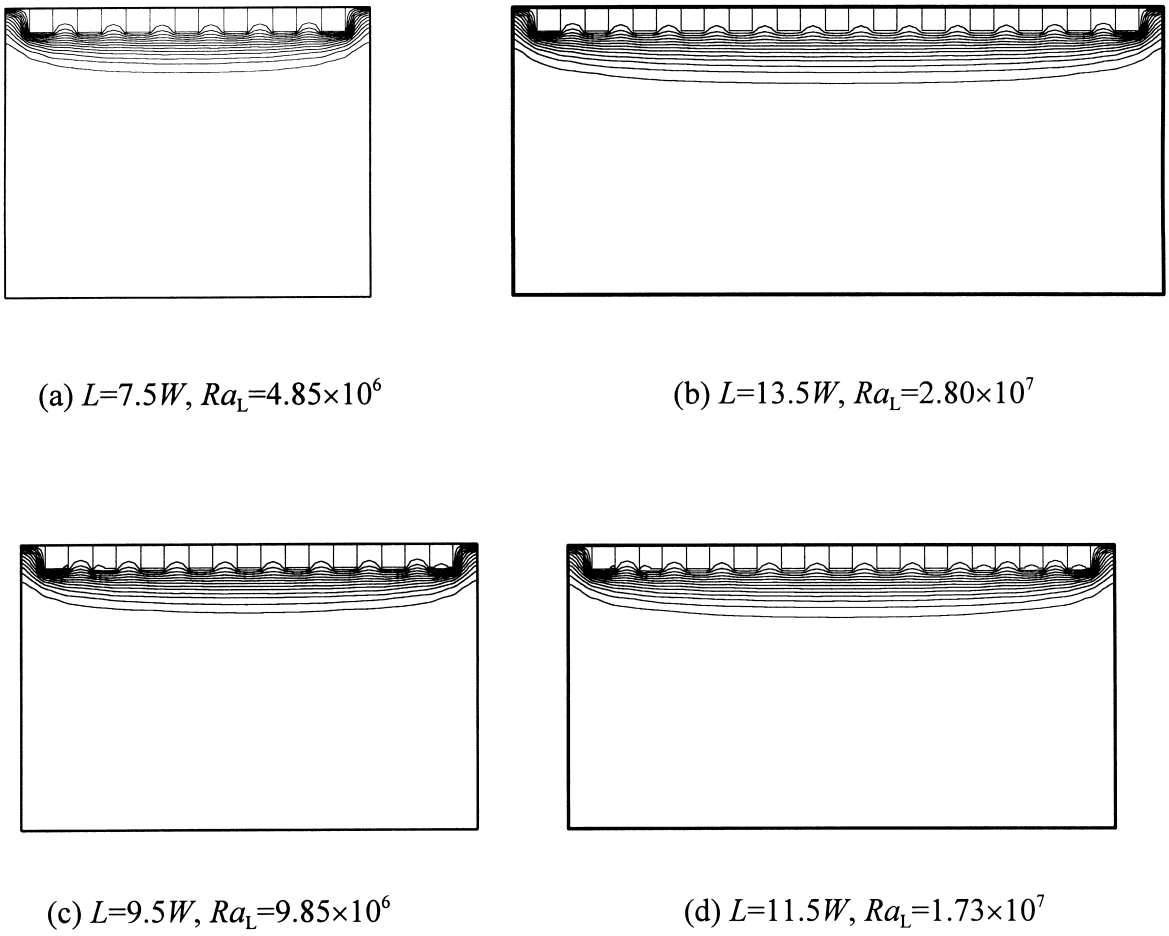

Fig. 9. Isotherms of square groove varying the number of protrusions ($Ra_W = 1.14 \times 10^4$).

The average Nusselt numbers are proportional to the 0.23 to 0.26th power of Rayleigh number, while that of a flat plate is obtained to be proportional to the 0.2th power. The ratio of Nusselt numbers averaged over five protrusions to the flat plate case is arranged as:

$$\overline{Nu}_{W,\mathrm{flat}} = 0.34 Ra_{\mathrm{W}}^{1/5} \quad \text{for flat plate}$$

$$\frac{\overline{Nu}_W}{\overline{Nu}_{W,\mathrm{flat}}} = 0.724 Ra_{\mathrm{W}}^{0.051} \quad \text{for case 1 (square groove)}$$

$$\frac{\overline{Nu}_W}{\overline{Nu}_{W,\mathrm{flat}}} = 0.882 Ra_{\mathrm{W}}^{0.03} \quad \text{for case 2 (shallow groove)}$$

$$\frac{\overline{Nu}_W}{\overline{Nu}_{W,\mathrm{flat}}} = 0.834 Ra_{\mathrm{W}}^{0.058} \quad \text{for case 3 (deep groove)}$$

$$\frac{\overline{Nu}_W}{\overline{Nu}_{W,\mathrm{flat}}} = 0.679 Ra_{W}^{0.05} \quad \text{for case 4 (wide groove).} \qquad (14)$$

A comment is appropriate here. The average Nusselt number $\overline{Nu}_W$ $(=\bar{h}W/k)$ has been defined to give the total heat transfer rate Q from the entire surface per unit depth as $\bar{h}L(T_{\mathrm{w}} - T_\infty)$. Note again that $L = 5.5W$. The first expression has been obtained from Eq. (13) by replacing L by $5.5W$.

The flow is laminar in the given range of Rayleigh number ($1.14 \times 10^4 \le Ra_W \le 1.14 \times 10^7$). However, the flow field is found to become unstable when Ra_W is greater than 1.14×10^7, which may indicate transition to turbulence.

When examining Eq. (14) carefully, we find that $\overline{Nu}_W$ is roughly proportional to the 0.25th power of Ra_W for the tested grooves. A more general correlation may be obtained by taking the 0.25th power of Rayleigh number and extending the correlation to general rectangular grooves and flat plates, and with more number of grooves. The following calculation is devised to estimate natural convection from that having more protrusions; natural convection from the plates having 7, 9, 11 and 13 protrusions for the four cases. In total, 33 cases are reviewed. The isotherms of square groove varying the number of protrusion are shown in Fig. 9. Quantitatively, the isotherms are the same as in the five-groove case. From the four tested geometries, the correlation is finally determined as,

$$\overline{Nu}_L = 0.27 \times \left(1 + 16.8 \frac{(H/W)^{1.45}(W/L)^{1.21}(W_2/W)^{0.33}}{1 + H/W}\right) Ra_L^{1/4} \qquad (15)$$

where L is total length of the plate. When the ratios $H/W, W/L, W_2/W$ approach to zero, Eq. (15) becomes,

$$\overline{Nu}_L = 0.27 Ra_L^{1/4}, \qquad (16)$$

an equation for a flat plate. Eq. (16) is an expression obtained by reforming Eq. (14) with the 0.25th power in the range of $10^6 \le Ra_L \le 10^9$. The maximum percentile error of correlation (15) is about 10%, and 95% of the data are within 3% error. Eq. (15) is recommended to use for $10^6 \le Ra_L \le 10^9$.

The experiments and analyses here have been made for air ($Pr = 0.71$). For future application to liquid cooling, correlations for other fluids are desirable. At this point, no precise prediction for fluids of different Pr can be made. However, it is anticipated that the present correlations may be used for other fluids without significant change, since, for example for laminar natural convection along a flat plate wall, the coefficient of the correlation between Nusselt number and Rayleigh number is only within 20% difference in the range of $0.7 \le Pr \le \infty$ [14].

6. Conclusion

Experimental and numerical studies on laminar natural convection from horizontal downward-facing plate with rectangular grooved fins have been performed. Both results agree well with each other for $Ra_W = 1.14 \times 10^4$, and the numerical method is further employed to investigate the heat transfer and flow field at different Ra_W. The Nusselt number is the greatest at the outer tip of the protrusion. At the left and the right side surfaces, it increases from the inner corner to the outer edge. It is very small at the upper surface of the groove; it has a local maximum at the center and decreases at the corners. At least one recirculation flow exists for all the tested cases in the groove. The protrusions prevent the main flow from flowing into the grooves. Consequently, the increase of the total heat transfer rate from grooved surface may not be sufficiently large especially when the Rayleigh number is not large enough. When Ra_W is large (roughly greater than 10^6), the heat transfer rate from the grooved fin becomes greater than that from a flat surface. The average Nusselt number over protrusions is roughly proportional to the 0.23–0.26th power of the Rayleigh number.

A very general correlation for the average Nusselt number is finally made to obtain the heat transfer rate for general rectangular grooves, for any number of protrusions and Rayleigh numbers.

Acknowledgements

The authors are grateful to Korea Science Foundation (Grant No. KOSEF 93-0600-02-3) and to Korean Ministry of Science and Technology (LM-01-02-A-02) for their financial support.

References

[1] E.J. Rymaszewski, R.R Tummala, Microelectronics packaging — an overview, in: Microelectronics Packaging Handbook, Nostrand Reinhold (Van), New York, 1989.
[2] F.P. Incropera, Convection heat transfer in electronic equipment cooling, ASME Journal of Heat Transfer 110 (1988) 1097–1111.
[3] R.C. Chu, R.E. Simons, Recent development of computer cooling technology, in: The Sixth International Symposium on Transport Phenomena, Seoul, Korea, 1993, pp. 17–25.
[4] A. Bejan, Geometric optimization of cooling techniques, in: S.J. Kim, S.W. Lee (Eds.), Air Cooling Technology for Electronic Equipment, CRC Press, Boca Raton, 1996 (Chapter 1).
[5] C.E. Kwak, T.H. Song, Experimental and numerical study on natural convection from vertical plates with horizontal rectangular grooves, International Journal of Heat and Mass Transfer 41 (16) (1998) 2517–2528.
[6] C.E. Kwak, T.H. Song, Experimental and numerical study on natural convection from upward horizontal rectangular grooved fins, in: InterSociety Conf. on Thermal Phenomena, I—THERM V, Orlando, USA, 1996, pp. 38–45.
[7] M. Fishenden, O.A. Saunders, An Introduction to Heat Transfer, Oxford University Press, London, 1961.
[8] V. Kadambi, R.M. Drake, Free convection heat transfer from horizontal surfaces for prescribed variations in surface temperature and mass flow through the surface, Technical Report Mech. Eng. HT-1, Princeton University (1960).
[9] T. Fujii, H. Imura, Natural convection heat transfer from a plate with arbitrary inclination, International Journal of Heat and Mass Transfer 15 (1972) 755–767.
[10] T. Aihara, Y. Yamada, S. Endo, Free convection along the downward-facing surface of a heated horizontal plate, International Journal of Heat and Mass Transfer 15 (1972) 2535–2549.
[11] W.N. Gill, D.W. Zeh, E. del Casal, Free convection on a horizontal plate, Zamp 16 (1965) 539–541.
[12] C. Wagner, Discussion on integral methods in natural convection flow, AIAA Journal of Applied Mechanics 23 (1956) 320–321.
[13] J.V. Clifton, A.J. Chapman, Natural convection on a finite-size horizontal plate, International Journal of Heat and Mass Transfer 12 (1969) 1573–1584.
[14] T. Fujii, H. Honda, I. Morioka, A theoretical study of natural convection heat transfer from downward-facing horizontal surfaces with uniform heat flux, International Journal of Heat and Mass Transfer 16 (1973) 611–627.
[15] F. Restrepo, L.R. Glicksman, The effect of edge conditions on natural convection from a horizontal plate, International Journal of Heat and Mass Transfer 17 (1974) 135–142.
[16] D.W. Hatfield, D.K. Edwards, Edge and aspect ratio effects on natural convection from the horizontal heated plate facing downwards, International Journal of Heat and Mass Transfer 24 (6) (1981) 1019–1024.
[17] R.J. Goldstein, K.S. Lau, Laminar convection from a horizontal plate and the influence of plate-edge extensions, Journal of Fluid Mechanics 129 (1983) 55–75.
[18] W. Hauf, U. Grigull, Optical methods in heat transfer, in: Advance in Heat Transfer, vol. 6, Academic Press, New York, 1970, pp. 191–278.
[19] S.V. Patankar, Numerical Heat Transfer and Fluid Flow, Hemisphere, New York, 1980.
[20] W.M. Rohsenow, J.P. Hartnett, E.N. Ganic, in: Handbook of Heat Transfer Fundamentals, 2nd ed., McGraw-Hill, New York, 1985.